# Passive radar delay and angle of arrival measurements of multiple acoustic delay lines used as passive sensors

W. Feng, J.-M Friedt, G. Goavec-Merou, M. Sato

*Abstract*—**After introducing noise radar probing of acoustic delay lines used as passive tags and sensors, we demonstrate the use of non-cooperative radiofrequency signal sources for such purposes in the context of passive radar measurement. A practical demonstration using IEEE 802.11n (WiFi) is given for a sensor operating at 2.42 GHz, solving the regulatory certification issue met when deploying dedicated radiofrequency emitters for short range radar applications. Furthermore, synthetic aperture radar measurement is completed by replacing the single surveillance antenna with a linear uniform array, solving the sensor collision issue when multiple targets are within range of the radar system.**

*Index Terms*—**SAW sensor, cooperative target, passive radar, WiFi, anti-collision, space division multiple access**

## I. INTRODUCTION

As we are constantly surrounded by electromagnetic smog, deploying wireless, passive sensors does not require developing new radiofrequency sources for probing the co-operative targets and monitoring their response: existing non-cooperative emitters might be well suited for such tasks, following the concepts of passive radar measurements [1]. Passive radar is widely used for monitoring static and moving targets: a reference channel collects an unknown signal emitted by a non-cooperative source, while a surveillance channel collects signals reflected by static and moving targets. The information gathered by such a system is limited to range, velocity and possibly azimuth and elevation in the case of arrays of the target(s). In this paper, we consider cooperative radar targets designed to return a signal representative of quantities characterizing their physical or chemical environment: sensors.

Acoustic transducers [3] (Fig. 1) have been shown to be well suited for designing passive, wireless sensors with no local energy source [4], [5], [6]. Their basic architecture only requires a single cleanroom lithography step since metallic electrodes patterned as interdigitated transducers [7] are deposited on a piezoelectric substrate. This piezoelectric substrate converts an incoming electromagnetic signal into a
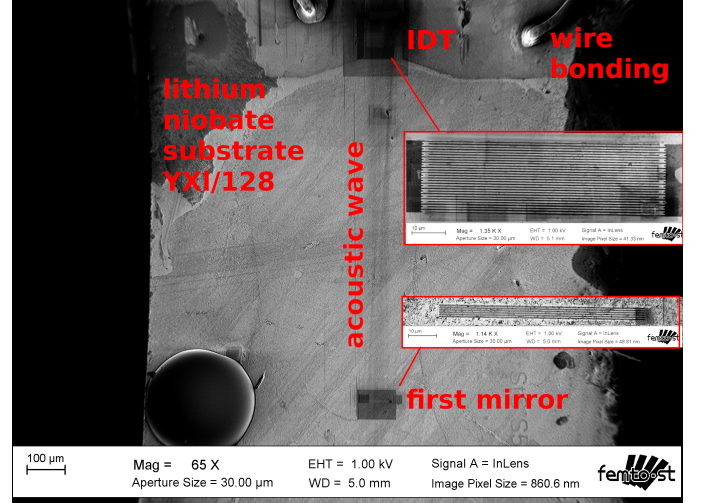
Fig. 1. Scanning Electron Microscope (SEM) image of an acoustic wave reflective delay line. The interdigitated transducers (IDT) are visible on the top of the image, the first mirror on the bottom, located in front of the other 7 mirrors not visible on the picture. A 15 dBm power at 2.4 GHz is injected in this device for the acoustic wave to be visible on the SEM image between the IDT and mirror [2]. This 1-mm long acoustic path induces a time delay of 0.5 $\mu$s considering the Rayleigh wave velocity of 4000 m/s on a lithium niobate YXl/128° substrate. The wire bondings connect the transducer to a ceramic package housing whose pads are soldered to an antenna for wireless probing.

surface acoustic wave (SAW) whose velocity is dependent on the surrounding physical properties of the transducer: the acoustic wave boundary conditions or piezoelectric substrate elastic modulus and density are dependent on properties such as temperature, stress or adlayer adsorption, hence yielding an echo delay dependence with such quantities. The acoustic wave is reflected by mirrors patterned on the piezoelectric substrate back to the electrodes converting the acoustic signal back to an electromagnetic wave, yielding a backscattered electromagnetic signal whose properties – resonance frequency or delay – are representative of a physical quantity under investigation. The conversion from electromagnetic to acoustic waves, the latter being $10^5$ times slower than the former, allows for compact implementation of delays well beyond clutter: the echoes introduced by the acoustic reflective delay lines are delayed by 1.0 to 2.5 $\mu$s, and yet the sensor dimensions remain only a few millimeter long thanks to the slow (typically 3000 to 5000 m/s [8]) acoustic wave. Delaying the echoes representative of the measurement beyond clutter improves the signal to noise ratio and lowers the requirements

on the elimination of the Direct Signal Interference (DSI), as will be shown in section III.

Such a wireless measurement system is, from a user perspective, reminiscent of Radio Frequency Identification (RFID) [9]. The underlying physical principles differ widely: while RFID backscatters an amplitude modulation through the antenna impedance variation – an intrinsically non-linear behavior – the SAW device delays the incoming electromagnetic signal beyond clutter in a tiny sensor benefiting from the slow acoustic wave with respect to the electromagnetic wave velocity. Furthermore, the linear piezoelectric electromechanical conversion allows for lower radiofrequency power to reach larger measurement range since no rectifier diode threshold voltage needs to be reached before powering the silicon based RFID.
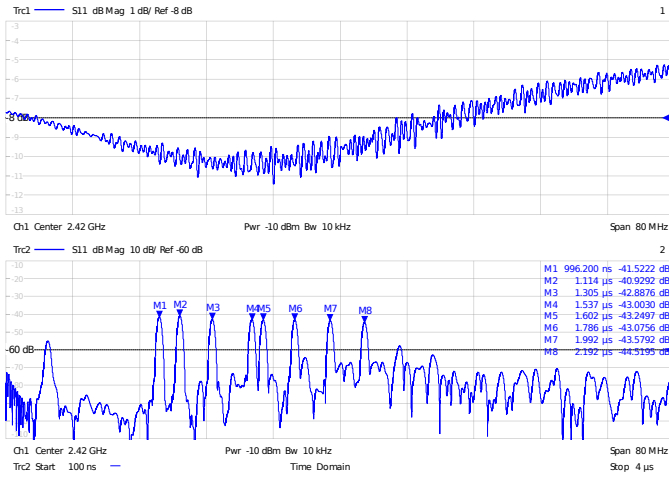


Fig. 2. Frequency domain (top) and time domain (bottom) reflection coefficient of the SAW delay line used for demonstrating passive radar interrogation of passive sensors.

Echo attenuation, representative of radar cross-section variation, is a typical measurement strategy for recovering the physical quantity sensed by the target [10]. However, radar cross-section measurement exhibits a poor resilience in practical applications due to the multiple causes of backscattered power variations, whether due to multipath interference, presence of absorbing obstacles or moving target varying the range and hence propagation losses. Examples of practical causes of varying boundary condition modifications include the impact of fluorescent lights on indoor link budgets [11], [12]: here, the absence or presence of ionized gas in the fluorescent light bulbs varies the microwave propagation path boundary conditions and hence the power returned to the receiver. The sensing capability is not significant beyond Tempest-like [13] attacks with little impact other than the remote detection that the lights are switched on. Indeed, while Tempest [14] monitors signals radiated by the electronic system being monitored, active extensions such as the National Security Agency's (NSA) [15] passive transducers generate a tuned response to impedance variations induced by the electronic system such as a keyboard or display screen cable being monitored, following the principles initially introduced by L. Theremin in his passive microphone [16]. More promising,

[17], [18], [19] demonstrate devices engineered to impact on the transmitted link budget through binary switches modifying again transmitted wave boundary conditions. As opposed to such approaches, throughout this paper we shall never consider amplitude as the measured quantity due to its strong sensitivity to environmental conditions and electromagnetic wave propagating boundary conditions, but shall always focus on the measurement of a time of flight (echo delay difference).

The SAW sensor industry is however neither as large nor organized as the RFID industry, and no radiofrequency band has been allocated to the short range radar systems used to probe SAW responses. As such, practical deployment of SAW readers [20], [21] are challenged when aiming at compliance with radiofrequency emissions, by attempting to fit within the Industrial, Scientific and Medical (ISM) unlicensed band certification requirements. An alternative to meet the requirements of certification is to divert existing radiofrequency emitters for probing SAW sensors, following a strategy similar to passive radar [22], [23], [1], in which a non-cooperative emitter signal is used beyond its original purpose to assess the delay of the reflected signals. Here we demonstrate such a concept by using SAW cooperative targets designed as tags and sensors.

Probing SAW sensors using passive radar requires non-cooperative source selection criteria more stringent than those classically used for target detection – namely broadband source for range resolution and high power to compensate for the losses rising as the fourth power of the monostatic radar equation, a particular case of the propagation losses determined by the product of the squared ranges from emitter to target and target to receiver. SAW sensors include two broad ranges of architectures: narrowband resonators and wideband reflective delay lines. The latter is designed to typically exhibit delays in the 1 to 2.5 $\mu$s range to delay the echoes beyond clutter and yet prevent excessive losses of the acoustic wave propagating over too long a path (Fig. 2). Including 8 bits within this time delay requires a time resolution of about 125 ns, or a bandwidth of 8 MHz. Practical separation of the echoes requires a bandwidth of about twice this frequency span, or about 16 MHz. Amongst the classical passive radar sources, broadcast FM stations are too narrowband with 250 kHz, Digital Video Broadcast-Terrestrial is hardly usable with 5 to 8 MHz bandwidth, while the 10 MHz GSM might be considered if a dedicated SAW transducer is designed with widely separated echoes.

Another aspect making SAW detection challenging is that all physical processes are linear, meaning that the returned signal is necessarily at the same frequency as the incoming electromagnetic signal, with attenuation and phase rotation of some spectral components defined by the reflection scattering coefficient as shown on Fig. 2. Hence, despite benefiting (by design) from clutter-free measurements in the time (range) domain, passive radar processing of stationary SAW transducer responses cannot benefit from the high signal to noise ratio of the Doppler-shifted echoes returned by moving targets. Furthermore, multiple targets within measurement range will simultaneously return power, leading to sensor response collision.

In this article, we will use the 15 MHz wide signal generated

by IEEE 802.11n transceivers, commonly labeled as WiFi. Such a signal will be used to probe commercial-off-the-shelf (COTS), SAW delay lines as obtained from Carinthian Tech Research (CTR, Villach, Austria): matching center frequency and bandwidth will make the identification of echoes possible when illuminating a SAW sensor with a WiFi signal and recovering on a digital oscilloscope both reference (emitted from the WiFi transceiver) and surveillance channels. However, before tackling the passive radar issue, we demonstrate first the noise-radar measurement of SAW sensor responses by synthesizing a pseudo-random source with appropriate center frequency and bandwidth matching the sensor spectral characteristics. Furthermore, adding a second delay line (provided by RSSI, Germany) operating in the same frequency band, spatial division multiple access (SDMA) is achieved for separating the two sensor responses by replacing the unique surveillance antenna with a linear, uniform linear array (ULA) allowing for identifying the direction of arrival of each signal.

## II. NOISE RADAR INTERROGATION OF SAW SENSORS

Before diverting existing radiofrequency emitters for bistatic passive radar demonstration, we assess the feasibility of measuring echo delays using noise-radar [24] (Fig. 3), thus demonstrating how selecting a radiofrequency source with the appropriate spectral characteristics allows for probing SAW sensor response. Indeed, the setup shown in Fig. 3 allows to independently tune the center frequency (local oscillator LO) and bandwidth by tuning the rate at which the Pseudo Random Number Generator (PRNG) is running. This preliminary experiment will provide the basic insight for selecting the non-cooperative source in a passive radar approach to probing SAW sensors.
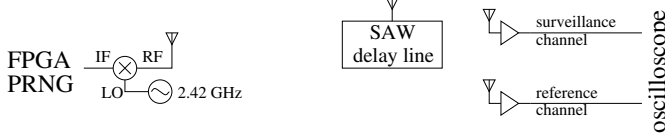


Fig. 3. Schematic of the noise radar experiment.

In this approach, the matched filter applied to the signal recorded by the radar receiver is a local copy of the pseudo-random sequence applied to a binary-phase shift keying (BPSK) encoded stream emitted towards the target. As is well known from Global Navigation Satellite System (GNSS) decoding [25], the pulse compression achieved by cross-correlating the returned signal including all the delayed copies of the emitted pseudo-random sequence yields correlation peaks whose width is given by the inverse bandwidth of the BPSK modulation.

In our practical demonstration, a 2.42 GHz carrier is phase modulated by feeding the Intermediate Frequency input of a mixer with a 20-bit long, 37 Mb/s Pseudo Random Sequence (PRNG) generated by the $x^{20}+x^3+1$ polynomial defining the taps of a Linear Feedback Shift Register (LFSR). The $2^{20}-1$ sample repetition rate of this Pseudo Random Sequence is 28 ms, defining the maximum pulse compression duration.
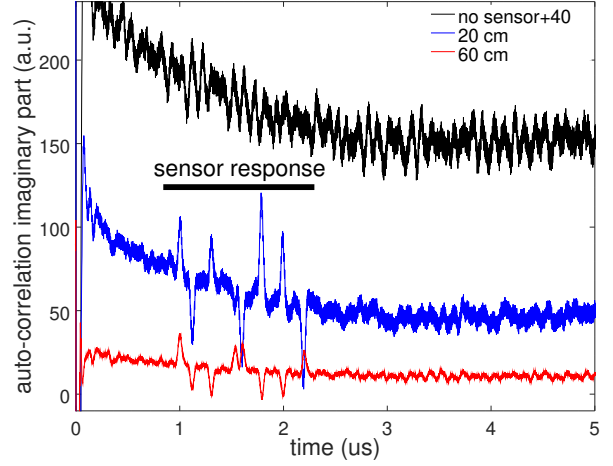


Fig. 4. Wireless measurement at a range of 0.2 and 0.6 m of a SAW delay line using a BPSK signal modulated by a 20-bit long pseudo-random sequence. The imaginary part of the cross-correlation is shown.

Rather than defining a dedicated reference channel, a single surveillance measurement is performed and *auto*correlation is computed since a strong component of the reference signal is recorded in addition to the sensor response (Fig. 4).

## III. WIFI BASED PASSIVE RADAR INTERROGATION OF SAW SENSORS

Having demonstrated the noise radar measurement of SAW sensors, we replace the dedicated source with a non-cooperative emitter made of an IEEE 802.11n emitter. Tuning to channel 3 yields a center frequency of 2.42 GHz and a 15 MHz wide signal, well suited to probing SAW delay lines.
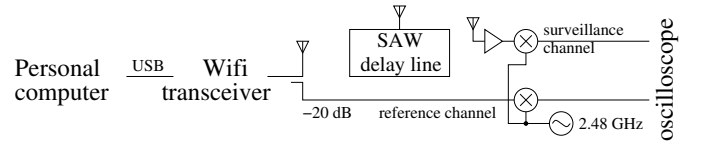


Fig. 5. Schematic of the passive radar experiment.

The experimental setup is as follows (Fig. 5):
1) a COTS WiFi transceiver (Alfa AWUS036NEH) is used as a signal source, set to channel 3 in Monitor mode,
2) the output of the WiFi transceiver is coupled (-20 dB, MiniCircuits ZX30-17-5-S+) to a mixer (Mini-Circuits ZEM-4300MH+) for downconversion with a 2.48 GHz reference signal (Rohde & Schwartz SMC100A, +13 dBm output). The reference signal is offset by 60 MHz from the WiFi channel 3 center frequency to prevent the transceiver from disconnecting if it detects excessive power in its operating radiofrequency band. The output of the coupler feeds one input of the oscilloscope labeled as reference channel,
3) the surveillance antenna is a directional cantenna [26] facing the sensor. The output of this horn antenna is amplified and feeds a mixer (MiniCircuits ZX05-63LH-S+) whose local oscillator input is connected to the same carrier as the one downconverting the reference signal.

Both mixer outputs are low pass filtered with a cutoff frequency of 600 MHz (Minicircuits SLP-600+).

All signals are collected using a LeCroy LabMaster 10-36ZiA oscilloscope at a rate of 250 MS/s to maximize the duration of the 125 MB records. Signal processing involves:

- selecting 8.4 ms ($2^{20}$ samples) long sub-set of the record to reduce the computational complexity,
- definition of a 60 MHz software oscillator, with 60 MHz the offset between the WiFi channel and the local oscillator used during the hardware downconversion,
- software frequency transposition to baseband by multiplying the signal with the local oscillator,
- short range ($<0.04$ $\mu$s) multipath signal removal – also known as DSI – using a least square method [27],
- cross-correlating the surveillance and reference signals.

Based on this analysis, the echoes are well visible at a bistatic range of up to 1.50 m (Fig. 6). However, this computation is only possible if time-delayed copies of the reference signal are removed from the surveillance measurement.
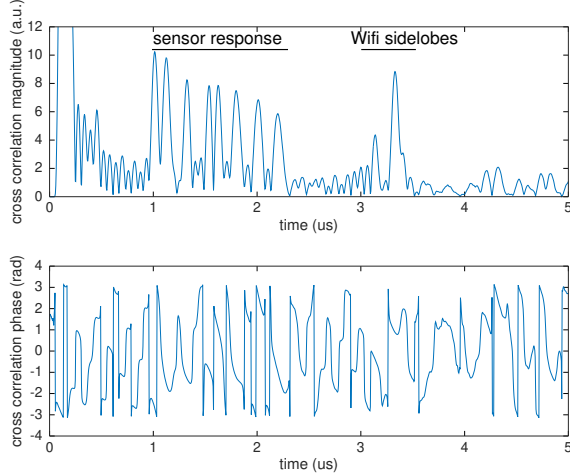


Fig. 6. Wireless measurement at a bistatic range of 1.05 m of a SAW delay line using an IEEE 802.11n signal. The sampling rate is 250 MS/s.

The most computationally intensive step is the DSI removal: computing the least square weights of the time delayed copies of the reference signal requires computing the pseudo-inverse matrix of time-delayed copies of the measurement signal. Considering the $2^{15}$ samples used to reach a sufficient signal to noise ratio during the cross-correlation computation, and the removal of the copies of the reference signal delayed by up to 64 ns (arbitrarily selected 19 m bistatic path), at a sampling rate of 250 MS/s (4 ns period) the matrix is 17 time-delay wide (0 to 16 samples). Handling such large matrices is practically not needed to identify the weights of the time delayed copies of the reference signal in the surveillance signal, and subsets as small as 4096 lines of the matrix containing the time-delayed copies have been used to identify the least-square method determined weights. Practically, we compute the DSI weights applied to each time delayed copy of the surveillance channel $surv$ as

$$DSI = (X^T \cdot X)^{-1} \cdot X^T \cdot surv$$

with $X = \begin{pmatrix} ref_1 & 0 & ... & 0 \\ ref_2 & ref_1 & ... & 0 \\ \vdots & \vdots & \ddots & 0 \\ ref_P & ref_{P-1} & ... & ref_{P-Q} \end{pmatrix}$

with $ref_i$ the samples from the reference channel, $P$ the number of samples and $Q$ the number of time delays to properly model the maximum range of the direct-path signal. $X$ is practically sub-sampled by selecting a random subset from the lines: reducing from $2^{15} \times 17$ to $4096 \times 17$ matrix size shrinks the computation time 10-fold with little impact on the time delays representing the sensor response, since only the short-delay weights are more poorly identified (Fig. 7).
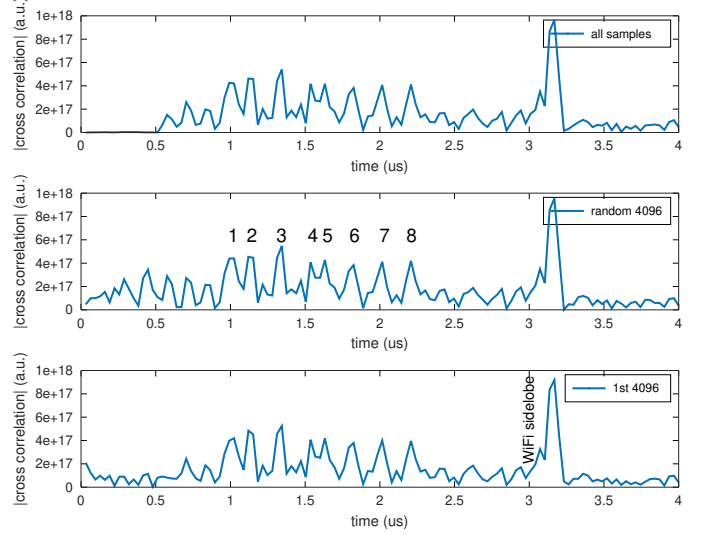


Fig. 7. Top: full DSI computation, with all $2^{15}$ reference channel samples and 17 time delays. Middle: DSI computation using a randomly selected subset of 4096 lines and keeping the same number of columns. Bottom: DSI computation using the first 4096 lines and keeping the same number of columns. Notice that the sensor response remain at the same in all cases, and only short delay contributions to the cross-correlation are improved by the full computation. The sampling frequency is here 31.2 MHz, so that removing the first 17 copies of the reference signal observed in the surveillance signal efficiently cancels the first 544 ns (top) clutter. The echoes ranging from 1 to 2.2 $\mu$s are indicated on the middle chart.

It is well known from delay line processing that the fine time of flight between echoes is best measured through the phase of the echoes [28]. While the absolute phase of each echo is dependent on the distance from radar to sensor as well as the acoustic velocity, the phase difference between returned echoes is solely dependent on the latter quantity. Since the acoustic velocity is dependent on the physical quantity under investigation, computing the phase of the returned echoes provides an estimate of this quantity. Since the correlation is a linear process, the phase is conserved and the phase of the echoes is transposed as the phase of the cross-correlation.

Computing the evolution of the phase as a function of time on multiple chunks of a given dataset collected for a bistatic range of 1.05 m, a standard deviation on the cross-correlation phase difference between the first two echoes separated by 112 ns is $d\varphi = 0.033$ rad. For a SAW delay line operating at $f = 2.42$ GHz, the phase introduced by a $\tau = 112$ ns delay is $\varphi = 2\pi f \cdot \tau = 1703$ rad. Considering the temperature

sensitivity of YXl/128° lithium niobate of $S = 70$ ppm/K, the temperature resolution achieved is $(d\varphi/\varphi)\cdot S^{-1} = 0.3$ K. Such a resolution is well within specifications of most temperature sensor applications in the context of industrial maintenance.
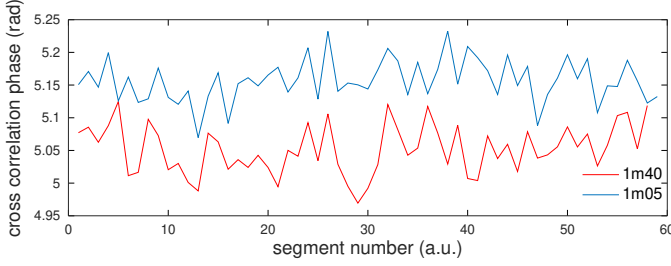


Fig. 8. Evolution of the phase of the cross correlation over time, for two measurements performed about 1 hour apart, with a bistatic range of 1.05 m and 1.40 m. Each segment lasts 8.4 ms so that each measurement duration is 500 ms.

The same measurement performed at a bistatic range of 1.4 m exhibits a standard deviation of the phase difference of 0.37 rad, but most importantly the mean value of this phase difference only differs by 0.10 rad between the two measurements (Fig. 8), accounting for a 1 K temperature estimate difference, well within range of the laboratory temperature evolution during the one hour-long duration of the experiment. This comparison hence demonstrates how the measurement is stable and insensitive to the geometrical configuration of the bistatic passive radar setup. In order to demonstrate the dynamic measurement of temperature, a 15 $\Omega$ power resistor is glued to the TO39 metallic can housing the sensing element fitted with a Pt100 reference probe. Fig. 9 demonstrates the excellent match between both measurements, with the wireless measurement performed at a bistatic range of 100 cm – 60 cm from the WiFi emitter to the sensor and 40 cm from sensor to the dipole receiver – considering a -76 ppm/K temperature sensitivity of lithium niobate and 0.3851 $\Omega$/°C for platinum. The piezoelectric substrate temperature sensitivity is well within the tabulated values for the YXl/128° cut of $70 \pm 10$ ppm/K [8]. The standard deviation on the stable temperature range at the beginning of the experiment of the phase is converted to a temperature standard deviation of 0.1 K. Since the temperature measurement is an analog measurement, the resolution is dependent on the signal to noise ratio and hence the link budget, degrading continuously as the range increases, but never collapsing suddenly as is the case with the digital communication of RFID systems. Computing the Allan deviation of the phase measurement exhibits a white noise and hence a standard deviation decrease as the square root of the integration duration. The current hardware implementation allows for 2 measurements/s.

## IV. ANTICOLLISION USING SPATIAL DIVISION MULTIPLE ACCESS

Signal collision is a classical issue for any communication system operating in the same frequency band, but emphasized for linear sensors which cannot benefit from non-linear modulation processes. While Time Division Multiple Access (TDMA) [29] and Code Division Multiple Access
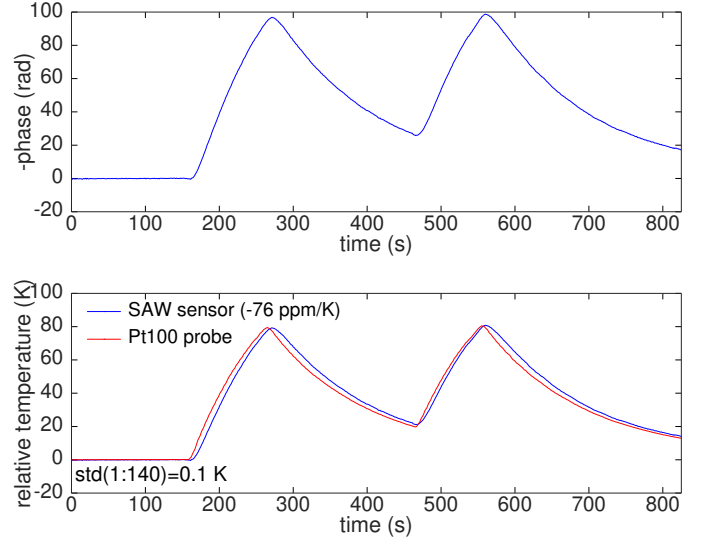


Fig. 9. Top: phase evolution of the first echo delayed by 1.05 $\mu$s as the temperature of the cooperative target first rises as a resistor glued to the sensor is heated, then cools, then rises again and finally cools back to room temperature. Bottom: conversion of the phase to temperature assuming a -76 ppm/K temperature sensitivity, and reference Pt100 probe temperature. The Pt100 probe is glued on the same resistor as the one used to heat the sensor.

(CDMA) have been investigated [30], [31], the limited encoding capability of SAW sensors related to the insertion loss rise due to multiple mirrors lying on the acoustic path prevents generalizing this approach. Here we focus on Spatial Division Multiple Access (SDMA) by replacing the single surveillance antenna with an ULA [32], [33]. The signal source remains the non-cooperative emitter, and each dipole antenna is sequentially connected to the surveillance channel following a processing strategy reminiscent of synthetic aperture radar [34]. Since the correlation is a linear process, the geometric phase introduced by the varying path length between sensor and receiving antenna is found in the correlation between the reference and surveillance signals. This phase will provide the information needed to identify the Direction of Arrival (DOA) in a far-field approximation of a plane wave reaching the antenna array from the sensor.

The practical demonstration is based on the two sensors characterized in the frequency domain (top) and time domain (bottom), emphasizing the collision of the echoes in frequency and time domains (Fig. 10).

The challenge of demonstrating time of arrival measurement, classically performed in synthetic aperture radar beamforming, is that two sources of delay here impact the observed echoes: on the one hand the geometric delay introduced by the geometric path between emitter and sensor and then sensor and receiver elements, and on the other hand the acoustic delay introduced by the delay line. The latter, in the microseconds range, is much longer than the former lying in the tens of nanoseconds range for sensor to antenna array distances in the meter range, practically observed as phase shift of the measured echoes since the range resolution $\delta r$ of the $B = 15$ MHz bandwidth signal is only $\delta r = c_0/(2B) = 10$ m with $c_0 = 300$ m/$\mu$s the velocity of the electromagnetic wave.
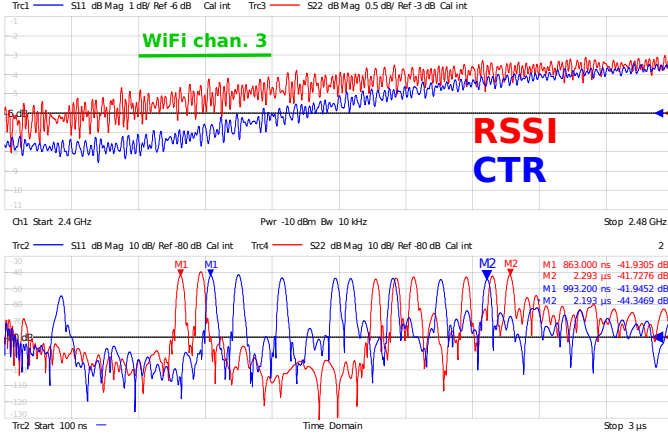
Fig. 10. Characterization of the CTR delay line uniformly spreading 8 echoes in the 1 to 2.3 $\mu$s range, and the RSSI delay line concentrating groups of echoes in the beginning and end of the message spanning the same time interval, yielding sensor response collision in both the frequency domain (top) and time domain (bottom).
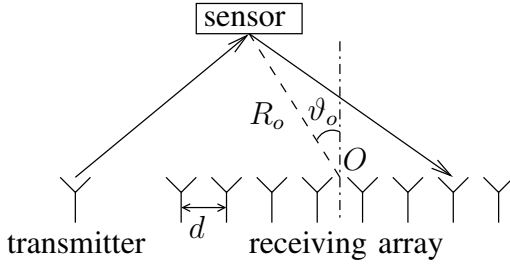


Fig. 11. Schematic of the experimental setup and notations used in deriving the signal processing algorithm.

Let us consider (Fig. 11) one spectral component of the signal emitted by the WiFi emitter – the demonstration can then be extended to any shape of emitted signal through its Fourier decomposition: the emitted signal is $s_0(t) = \cos(2\pi f_m t)$. Assuming an ULA with a spacing $d$ between elements, then the signal received by the $n$th antenna is expressed as

$$s_{surv}^n(t) = \sum_{p=1}^{P} s_o(t - \tau_{p,n})$$

where $\tau_{p,n}$ is the delay introduced by the $p$th reflector of a sensor as the sum of the acoustic delay $\tau_p$ intrinsic to the delay line sensor and the geometric delay

$$\frac{1}{c_0}\sqrt{(R_o \sin(\vartheta_o) - x_n)^2 + R_o^2 \cos^2(\vartheta_o)}$$

with $\{R_o, \vartheta_o\}$ the range and polar angle defining the position of the sensor with respect to the array, valid for all $n = 1, ..., N$ receiver elements of the $N$-antenna array.

In order to optimized the measurement bandwidth and maximize measurement duration for a finite memory depth of the recording system, a downconverter mixing stage followed by a low-pass filter are used prior to recording the radiofrequency signal: assuming a local oscillator $f_{LO}$, then the reference signal becomes

$$s_{ref}(t) = s_0(t) \cdot \cos(2\pi f_{LO} t) \propto \cos(2\pi(f_{LO} - f_m)t)$$

after removing, thanks to the low-pass filter, the frequency sum term. Similarly, after downconverting and low-passfiltering, the surveillance signal at the $n$th antenna becomes

$$s_{surv}^n(t) = \sum_{p=1}^{P} \cos(2\pi(f_{LO} - f_m)t + 2\pi f_m \tau_{p,n})$$

The collected real data are moved to baseband and converted to analytical signals thanks to the Hilbert transform to yield

$$s_{ref}(t) = \exp(j2\pi(f_{LO} - f_{base} - f_m)t)$$

with $f_{base} = f_{LO} - f_0$ and

$$s_{surv}^n = \sum_p \exp(j2\pi(f_{LO} - f_{base} - f_m)t + f_m \tau_{p,n})$$

The Fourier transform of the cross-correlation obtained as the product of the Fourier transform of the reference measurement channel multiplied by the complex conjugate of the Fourier transform of each surveillance channel yields

$$S_{cc}^n(f_m) = S_{surv}^n(f_m) \cdot S_{ref}^{*}(f_m) = \exp(j2\pi f_m \tau_n)$$

In the far field assumption, which is here used to simplify the demonstration but is not restrictive to an extension removing the following approximation, we consider $R_o \gg L^2/\lambda$ where $L$ is the antenna array length and $\lambda = c_0/f_0$ is the received signal wavelength, so that

$$\sqrt{(R_o \sin \vartheta_o - x_n)^2 + R_o^2 \cos^2(\vartheta_o)} \simeq R_o - x_n \sin(\vartheta_o)$$

resulting in

$$S_{cc}^n(f_m) \simeq \exp\left(j2\pi f_m(\tau_p + (R_o - x_n \sin(\vartheta_0))/c_0)\right)$$

or to isolate the dependence with the antenna index, considering $\tau_o = R_o/c_0$:

$$S_{cc}^n(f_m) \simeq \exp\left(j2\pi f_m(\tau_p + \tau_o)\right) \cdot \exp\left(j2\pi f_m x_n \sin(\vartheta_0)/c_0\right)$$

Discretizing this equation to consider the $m$-th frequency around $f_0$ so that $f_m = f_0 + m\Delta f$, then

$$S_{cc}(m, n) = \exp\left(j2\pi f_m(\tau_p + \tau_o)\right) \cdot \exp\left(j2\pi f_0 x_n \sin(\vartheta_0)/c_0\right)$$
$$\cdot \exp\left(j2\pi m\Delta f x_n \sin(\vartheta_0)/c_0\right)$$

According to [35], the last term of the last equation can be discarded if $2\pi m\Delta f x_m \sin(\vartheta_o)/c_0 \ll \pi/2$: this condition is satisfied assuming that

$$\max\{2\pi m\Delta f x_n \sin(\vartheta_0)/c\} = 2\pi \frac{B}{2} \cdot \frac{L}{2c_0} = \frac{\pi}{2} \cdot \frac{L}{c_0/B} \ll \frac{\pi}{2}$$

yielding $\frac{L}{\delta r} \ll 1$. We have seen earlier that $\delta r = 10$ m while in our experimental setup of 8 antennas separated by $\lambda/2$ we have $L \simeq 44$ cm (Fig. 12), satisfying the approximation.

Therefore, using $c_0/f_0 = \lambda_0$,

$$S_{cc}(m, n) \simeq \exp\left(j2\pi f_m(\tau_p + \tau_o)\right) \cdot \exp\left(j2\pi x_n \sin(\vartheta_0)/\lambda_0\right)$$

This expression emphasizes that $S_{cc}$ is the product of two inverse Fourier transforms, one in the range direction $F_1$ and the other in the azimuth direction $F_2$: using the two-dimensional inverse Fourier transform yields the range-azimuth map

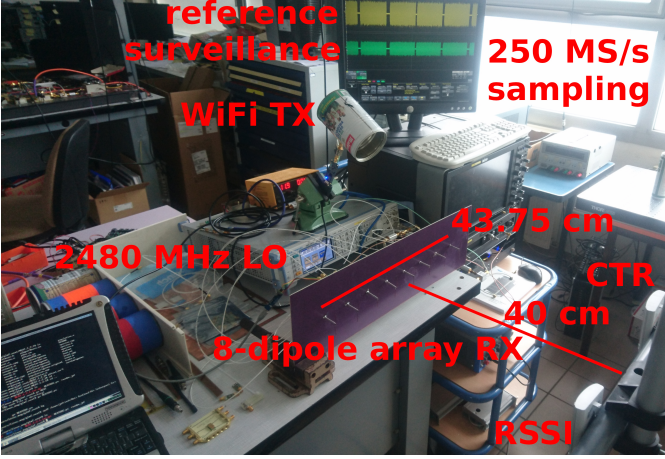$$\chi(\tau, \vartheta) = F_1 \cdot S_{cc} \cdot F_2^{*}$$

Fig. 12. Experimental setup for the ULA measurement allowing for spatial discrimination of sensor responses.

The result of this computation is exhibited in Fig. 13. We emphasize that throughout this calculation, the position of the emitter is undefined and that the intrinsic time delay introduced by the acoustic sensors do not appear in the azimuth compression. Hence, as can be seen in Figs. 13 or 14, all the acoustic echoes align beyond the given azimuthal angle defining the angular position of the sensor with respect to the array.

## V. CONCLUSION

Noise-radar measurement of Surface Acoustic Wave reflective delay lines acting as passive, wireless cooperative targets, is demonstrated with fine control of spectral occupation by separating the center frequency carrier from the spectral spreading capability of binary phase shift keying encoding a pseudo-random sequence. Based on this preliminary demonstration of noise radar, the principle is extended to a passive radar using a non-cooperative WiFi emitter with a single channel illuminating a surface acoustic wave sensor. The physical quantity impacting on the acoustic velocity and hence the time delay of the echo is recovered by analyzing the phase of the echoes computed as the cross-correlation between the reference and surveillance channels. Measurement distances in the couple of meters bistatic range and temperature resolution in the sub-K range are demonstrated using such a setup, solving the challenge of short range radar system certification for probing SAW devices acting as cooperative targets. Finally, sensor response collision issues are solved by angular separation of their echoes by replacing the unique surveillance antenna by a uniform linear array of 8 dipoles, allowing for direction of arrival measurement of the incoming signal and hence spatial separation of the responses. The measurement range is determined by the number of samples collected defining the pulse compression ratio and hence the signal to noise ratio improvement. However, direct signal interference is a major hindrance in the passive radar approach due to the intrinsic correlation in the emitted waveform: the delayed copies of the reference signal in the surveillance datasets are subtracted following a least-square identification.
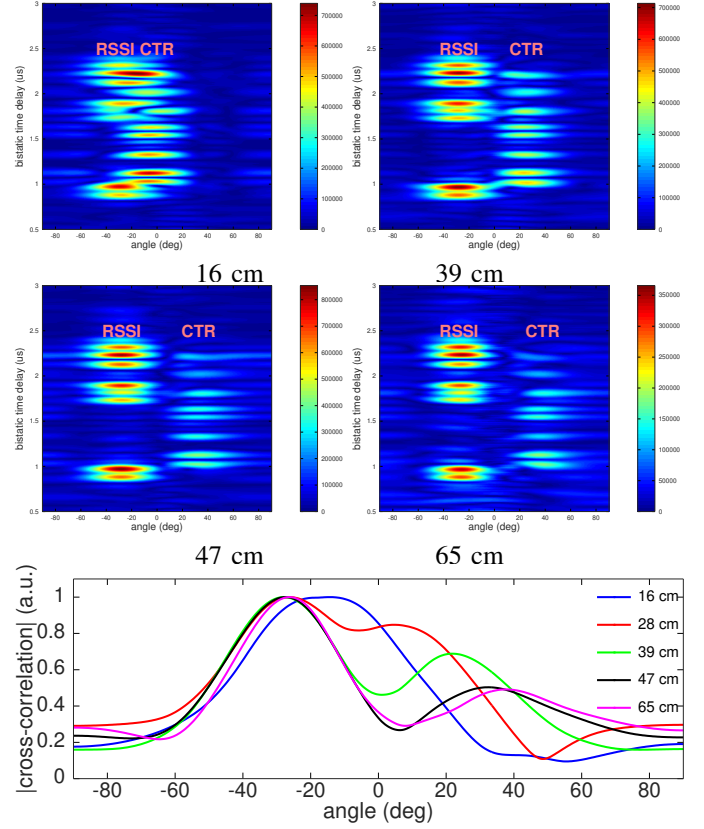


Fig. 13. Top: range-azimuth maps of two sensors measured using an ULA of 8 dipole antennas illuminated by a WiFi emitter, with varying distance between sensors. Bottom: range-compressed azimuthal distribution of returned power exhibiting the ability to separate sensors when spaced by more than 28 cm.
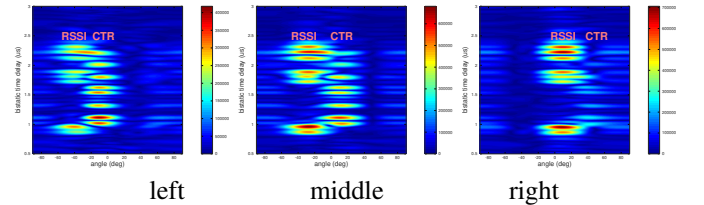


Fig. 14. Range-azimuth map of two sensors measured using an ULA of 8 dipole antennas illuminated by a WiFi emitter, keeping the distance between sensors constant at 28 cm but moving the sensor pair with respect to the array center.

Current improvements aim at increasing the measurement rate by replacing the oscilloscope with an embedded acquisition system, including the frequency transposition and filtering in the field programmable gate array in charge of the data sampling and pre-processing. By further reducing the number of samples in the least square identification as demonstrated in this paper, the acquisition and processing duration has been reduced to 0.5 s, well within temperature measurement update rates compatible with most industrial applications. Further improvement on the measurement update rate is desirable for applications aimed at strain sensing where modal analysis requires typical refresh rates in the kilosamples/s, hence requiring further improvement on the data processing duration.

REFERENCES

[1] H. D. Griffiths and C. J. Baker, *An Introduction to Passive Radar*. Artech House, 2017.

[2] A. Godet, J. Friedt, S. Dembélé, N. Piat, A. Khelif, P. Vairac, J. Agnus, P. Bourgeois, and G. Goavec-Mérou, "Mapping acoustic field distributions of VHF to SHF SAW transducers using a scanning electron microscope," in *European Frequency and Time Forum (EFTF), 2016*. IEEE, 2016, pp. 1–4.

[3] V. P. Plessky and L. M. Reindl, "Review on SAW RFID tags," *IEEE transactions on ultrasonics, ferroelectrics, and frequency control*, vol. 57, no. 3, 2010.

[4] W. Buff, F. Plath, . Schmeckebier, M. Rusko, T. Vandahl, H. Luck, F. Möller, and D. Malocha, "Remote sensor system using passive SAW sensors," in *IEEE Ultrasonics Symposium*, 1994, pp. 585–588.

[5] A.Pohl, F.Seifert, L.Reind, G.Scholl, T. Ostertag, and W.Pietschl, "Radio signals for SAW ID tags and sensors in strong electromagnetic interference," in *IEEE Ultrasonics Symposium*, 1994, pp. 195–198.

[6] M. Lamothe, V. Plessky, J.-M. Friedt, T. Ostertag, and S. Ballandras, "Ultra-wideband SAW sensors and tags," *Electronics Letters*, vol. 49, no. 24, pp. 1576–1577, 2013.

[7] R. White and F. Voltmer, "Direct piezoelectric coupling to surface elastic waves," *Applied physics letters*, vol. 7, no. 12, pp. 314–316, 1965.

[8] D. Morgan, "Surface acoustic wave filters," *Amsterdam: Elsevier*, 2007.

[9] I. Zalbide, E. D'Entremont, A. Jimenez, H. Solar, A. Beriain, and R. Berenguer, "Battery-free wireless sensors for industrial applications based on UHF RFID technology," in *SENSORS, 2014 IEEE*. IEEE, 2014, pp. 1499–1502.

[10] M. M. Jatlaoui, F. Chebila, S. Bouaziz, P. Pons, and H. Aubert, "Original identification technique of passive em sensors using loaded transmission delay lines," in *Microwave Conference (EuMC), 2010 European*. IEEE, 2010, pp. 1106–1109.

[11] P. Melangon and J. Lebel, "Effects of fluorescent lights on signal fading characteristics for indoor radio channels," *Electonics Letters*, vol. 28, no. 18, pp. 1740–1741, August 1992.

[12] G. Ibrahim, J. Sensening, and T. Al-Mahdawi, "Dynamic reflection of RF signals from fluorescent lights: Their spectral analysis and effects on backscattered RFID tag signals," in *IEEE Sarnoff Symposium*, Princeton, NJ, USA, 2007.

[13] W. Van Eck, "Electromagnetic radiation from video display units: An eavesdropping risk?" *Computers & Security*, vol. 4, no. 4, pp. 269–286, 1985.

[14] M. G. Kuhn and R. J. Anderson, "Soft tempest: Hidden data transmission using electromagnetic emanations," in *International Workshop on Information Hiding*. Springer, 1998, pp. 124–142.

[15] J. Appelbaum, J. Horchert, and C. Stöcker, "Shopping for spy gear: Catalog advertises nsa toolbox," *Der Spiegel*, 12/29/2013, leaksource. info/2013/12/30/nsas-ant-division-catalog-of-exploits-for-nearly.

[16] A. Glinsky, *Theremin: Ether Music And Espionage*. University of Illinois Press, 2005.

[17] B. Kellogg, V. Talla, S. Gollakota, and J. R. Smith, "Passive Wi-Fi: Bringing low power to Wi-Fi transmissions," in *NDSI*, vol. 16, 2016, pp. 151–164.

[18] B. Kellogg, A. Parks, S. Gollakota, J. R. Smith, and D. Wetherall, "Wi-Fi backscatter: Internet connectivity for RF-powered devices," in *SIGCOMM'14*, Chicago, IL, USA, August 2014.

[19] V. Iyer, J. Chan, and S. Gollakota, "3D printing wireless connected objects," in *ACM Transactions on Graphics*, vol. 36, no. 6, November 2017, p. 242.

[20] A. Stelzer, S. Schuster, and S. Scheiblhofer, "Readout unit for wireless SAW sensors and ID-tags," in *International Workshop on SiP/SoC Integration of MEMS and Passive Components with RF-ICs*, 2004.

[21] F. Lurz, T. Ostertag, B. Scheiner, R. Weigel, and A. Koelpin, "Reader architectures for wireless surface acoustic wave sensors," *Sensors*, vol. 18, no. 6, p. 1734, 2018.

[22] H. Guo, S. Coetzee, D. Mason, K. Woodbridge, and C. Baker, "Passive radar detection using wireless networks," in *IET International Conference on Radar Systems*, Edinburgh, UK, 2007.

[23] K. Chetty, G. E. Smith, and K. Woodbridge, "Through-the-wall sensing of personnel using passive bistatic wifi radar at standoff distances," *IEEE Transactions on Geoscience and Remote Sensing*, vol. 50, no. 4, pp. 1218–1226, 2012.

[24] J. R. Humphries, F. K. Reed, C. P. Carmichael, P. L. Fuhr, T. J. McIntyre, A. R. Weeks, and D. C. Malocha, "Noise radar approach for interrogating SAW sensors using software defined radio," *IEEE Sensors Journal*, vol. 17, no. 20, pp. 6760–6769, 2017.

[25] K. Borre, D. M. Akos, N. Bertelsen, P. Rinder, and S. H. Jensen, *A software-defined GPS and Galileo receiver: a single-frequency approach*. Springer Science & Business Media, 2007.

[26] G. L. Charvat, *Small and short-range radar systems*. CRC Press, 2014.

[27] F. Colone, R. Cardinali, and P. Lombardo, "Cancellation of clutter and multipath in passive radar using a sequential approach," in *Radar, 2006 IEEE Conference on*. IEEE, 2006, pp. 7–pp.

[28] Z. Zheng, T. Han, and P. Qin, "Maximum measurement range and accuracy of SAW reflective delay line sensors," *Sensors*, vol. 15, no. 10, pp. 26 643–26 653, 2015.

[29] A. Pohl, G. Ostermayer, L. Reindl, and F. Seifert, "Spread spectrum techniques for wirelessly interrogable passive SAW sensors," *IEEE Fourth International Symposium on Spread Spectrum Techniques and Applications*, pp. 730–735, 1996.

[30] C. Hartmann, P. Hartmann, P. Brown, J. Bellamy, L. Claiborne, and W. Bonner, "Anti-collision methods for global SAW RFID tag systems," in *Ultrasonics Symposium, 2004 IEEE*, vol. 2. IEEE, 2004, pp. 805–808.

[31] M. Brandl, S. Schuster, S. Scheiblhofer, and A. Stelzer, "A new anti-collision method for SAW tags using linear block codes," in *IEEE International Frequency Control Symposium - Honolulu, HI*, 2008. [Online]. Available: http://gen.lib.rus.ec/scimag/index.php?s=10. 1109/FREQ.2008.4623005

[32] A. Stelzer, S. Scheiblhofer, S. Schuster, and M. Brandl, "Multi reader/multi-tag SAW RFID systems combining tagging, sensing, and ranging for industrial applications," in *Frequency Control Symposium, 2008 IEEE International*. IEEE, 2008, pp. 263–272.

[33] C. Pfeffer, S. Scheiblhofer, R. Feger, and A. Stelzer, "An s-fscw based multi-channel reader system for beamforming applications using surface acoustic wave sensors." *Radioengineering*, vol. 20, no. 4, 2011.

[34] L. M. Ulander, P.-O. Frölind, A. Gustavsson, R. Ragnarsson, and G. Stenström, "Airborne passive sar imaging based on dvb-t signals," in *Geoscience and Remote Sensing Symposium (IGARSS), 2017 IEEE International*. IEEE, 2017, pp. 2408–2411.

[35] J. Fortuny-Guasch, "A fast and accurate far-field pseudopolar format radar imaging algorithm," *IEEE Transactions on Geoscience and Remote Sensing*, vol. 47, no. 4, pp. 1187–1196, 2009.